RESEARCH ARTICLE | JUNE 12 2019

Dynamic susceptibility of modulated magnetic nanowires

Eduardo Saavedra; Guidobeth Saez ; Pablo Díaz; Eduardo Cisternas; Eugenio E. Vogel; Juan Escrig

AIP Advances 9, 065007 (2019)
https://doi.org/10.1063/1.5091813

Dynamic susceptibility of modulated magnetic nanowires

Cite as: AIP Advances 9, 065007 (2019); doi: 10.1063/1.5091813
Submitted: 5 February 2019 • Accepted: 30 May 2019 •
Published Online: 12 June 2019

Eduardo Saavedra,[1] Guidobeth Saez,[2] Pablo Díaz,[2] Eduardo Cisternas,[2] Eugenio E. Vogel,[2,3] and Juan Escrig[1,3,a)]

AFFILIATIONS

[1]Departamento de Física, Universidad de Santiago de Chile (USACH), Av. Ecuador 3493, 9170124 Santiago, Chile
[2]Departamento de Ciencias Físicas, Universidad de La Frontera, Casilla 54-D, 4811186 Temuco, Chile
[3]Center for the Development of Nanoscience and Nanotechnology (CEDENNA), 9170124 Santiago, Chile

[a)]E-mail: juan.escrig@usach.cl

ABSTRACT

We have calculated the dynamic susceptibility of modulated permalloy nanowires of 1-μm long and 50 nm diameter using micromagnetic simulations. The resonance modes obtained from these simulations are investigated as functions of both the position of the modulation along the nanowire as well as the size of it. The results presented in this work are important in view of the possible realization of tunable frequency magnonic devices, since we showed that it is possible to adjust a set of frequencies by controlling the geometric parameters of the system.

I. INTRODUCTION

Magnetic nanowires can potentially participate in new applications such as sensors,[1] logic or spintronics devices (e.g., spin valves, magnetic tunnel junctions), biomedical applications and three-dimensional recording systems (e.g., racetrack memories), where the data is stored vertically instead of longitudinally.[2] In addition, magnetic nanowires can be used as permanent magnets, because they exhibit a strong shape anisotropy that produces an increase in the coercivity of the system.[3] Additionally, it has been demonstrated that the domain walls in cylindrical nanowires, local deformations of the magnetization that separate two uniform and opposite magnetic domains, and that can be transverse or vortex,[4] can reach very high propagation speeds, because they do not exhibit the Walker breakdown.[5]

If one would like to effectively use these magnetic nanowires in one of the potential applications mentioned above, it is necessary to control with high precision both the position and velocity of propagation of the domain walls, which can be achieved using diameter modulated nanowires.[6–15] It has been experimentally demonstrated that the modulations have a strong influence on the magnetic properties of the system due mainly to an increase of the dipolar field in the vicinity of the modulation of the nanowire due to the accumulation of magnetic charges.[16,17] In addition, nanowires with periodic geometrical constrictions have been proposed to control the transmission bandgap characteristics of spin waves. In this way, diameter-modulated nanowires emerge as a three-dimensional engineering response to control the pinning/depinning process of the domain walls.

On the other hand, the ferromagnetic resonance (FMR) frequency of the nanowires generally shows two main peaks.[18,19] The high frequency peak has an absorption frequency that depends on the aspect ratio of the wire. This feature suggests the use of these nanowires as adjustable microwave filters. In addition, arrays of nanowires composed of different materials and exhibiting different aspect ratios can be used as comb filters. In this way, if the nanowires are interesting, it is expected that by investigating the dynamic behavior of nanowires with modulated diameters, they can be used for magnetic recording applications or microwaves devices. To achieve short reversion times, a high cutoff frequency of the real part of the dynamic susceptibility is required.[20] Finally, both the shape of the imaginary part of the susceptibility and the frequency position of the resonances are also important.

It is well known that in order to calculate the magnetic susceptibility of an arbitrary magnetization pattern, micromagnetic simulations are developed.[19–28] In this paper, micromagnetic

simulations have been performed in order to gain insight into the dynamic susceptibility for 1 μm long cylindrical nanostructures with modulated diameters at different positions along the axis. We have considered permalloy nanowires because it is a soft alloy that exhibits a negligible magnetocrystalline anisotropy, so that we can focus our attention on the way the geometrical parameters determine the dynamic response of these systems.

II. MICROMAGNETIC SIMULATIONS

The magnetization dynamics is governed by the Landau–Lifshitz–Gilbert equation (LLG)[29]

$$\frac{d\boldsymbol{M}}{dt} = -\gamma \boldsymbol{M} \times \boldsymbol{H}_{eff} + \frac{\alpha}{M_s}\boldsymbol{M} \times \frac{d\boldsymbol{M}}{dt} \quad (1)$$

where γ is the gyromagnetic ratio of the free electron spin and α is a phenomenological damping constant. The equation describes both the precession and relaxation motion of the magnetization in an effective field $\boldsymbol{H}_{eff}$. The calculations were performed using Oriented MicroMagnetic Framework software (OOMMF),[30] which uses an iterative process to solve the Landau-Lifshitz equation using the finite differences method.[31]

The simulated nanowires were permalloy ($Ni_{80}Fe_{20}$) of 1-μm in length and 50 nm in diameter. We consider three cases: a single nanowire (SW), a wide modulated nanowire (WMN) with a modulation of 100 nm in thickness and 100 nm in diameter, and a narrow modulated nanowire (NMN) also with a modulation of 100 nm in thickness, but with a diameter of 30 nm (see Fig. 1). For permalloy material, the exchange stiffness, A, was set at 13×10^{-12} J/m, and the material saturation magnetization, Ms, was set to 800×10^3 A/m.[20] Polycrystalline samples were considered, so the magnetocrystalline anisotropy was not taken into account. The samples were discretized into a cell size of $2 \times 2 \times 5$ nm^3 (the latter along the cylindrical axis). The damping coefficient of the Landau-Lifshitz equation was set to 0.015 because it is the value commonly used for to simulate Permalloy (see, for example, Refs. 18, 19, 21, 22, 26, and 32). It was assumed that the wire–wire distance is large enough to consider every wire as independent.

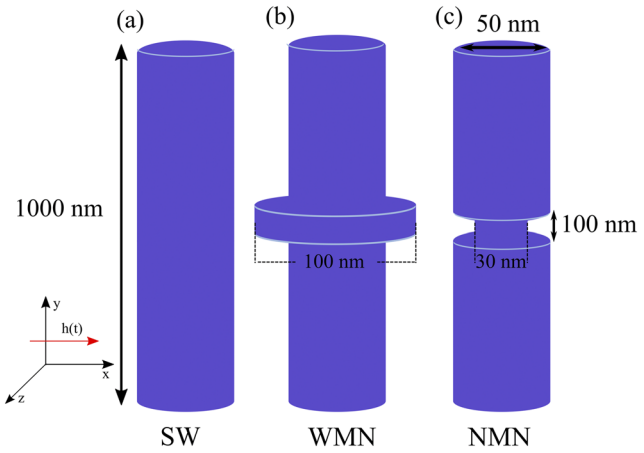

FIG. 1. Geometrical parameters for the simulated nanowires: (a) a single nanowire (SW), (b) a wide modulated nanowire (WMN) and (c) a narrow modulated nanowire (NMN).

The idea is to study the resonance modes as a function of the position of these modulations along the nanowire via micromagnetics. The magnetization distribution of the ground state is obtained by the minimization of the total energy density functional $\boldsymbol{E} = \boldsymbol{E}_{\text{exchange}} + \boldsymbol{E}_{\text{demag}} + \boldsymbol{E}_{\text{anisotropy}} + \boldsymbol{E}_{\text{Zeeman}}$. The average energy density E is a function of $\boldsymbol{M}(\boldsymbol{r}, \boldsymbol{t})$ specified by Brown's equations including exchange, self-magnetostatic (demagnetization), anisotropy, and applied field (Zeeman). The equilibrium configurations for five different positions of the modulations (550 nm, 650 nm, 750 nm, 850 and 950 nm), for both the WMN and the NMN, are shown in Fig. 2. The structures exhibit a quasiuniform single-domain state in which the magnetization is mainly oriented along the symmetry axis, except within the modulation for the WMN, which stabilizes a vortex. After the equilibrium magnetization was obtained, the dynamic susceptibility is determined by computing the response of the magnetization configuration to a weak magnetic excitation, $\boldsymbol{h}(\boldsymbol{t}) = \boldsymbol{1000exp}\left(-\boldsymbol{10^9 t}\right)(\boldsymbol{t} \geq \boldsymbol{0})$,[19,23,27] applied uniformly and perpendicular to the long axis of the modulated nanowire (see Fig. 1). Here, $\boldsymbol{h}(\boldsymbol{t})$ is in A m^{-1} and t is in seconds. The amplitude of the pulse field was small enough to remain in the linear response region.[33] The evolution of the magnetization under the exciting field was collected for 3 ns by saving the magnetization configuration at uniform time intervals of 1 ps. The small exciting magnetic field $\boldsymbol{h}(\boldsymbol{t})$ and the magnetization distribution $\boldsymbol{M}(\boldsymbol{r}, \boldsymbol{t})$ were transformed to the frequency domain $[\boldsymbol{h}(\boldsymbol{\omega}), \boldsymbol{M}(\boldsymbol{\omega})]$ by using the fast Fourier transform (FFT) method, respectively. Complex magnetic susceptibility $\left(\boldsymbol{\chi} = \boldsymbol{\chi}' - \boldsymbol{j\chi}''\right)$ can be calculated by $\boldsymbol{\chi}(\boldsymbol{\omega}) = \boldsymbol{M}(\boldsymbol{\omega})/\boldsymbol{h}(\boldsymbol{\omega})$. The imaginary part of the susceptibility $\left(\boldsymbol{\chi}''\right)$ was computed by dividing the Fourier transform of the response $[\boldsymbol{M}(\boldsymbol{\omega})]$ by the Fourier transform of the excitation $[\boldsymbol{h}(\boldsymbol{\omega})]$.[34]

III. RESULTS AND DISCUSSION

A. Wide modulated nanowire (WMN)

The dynamic susceptibility curves for a WMN with a modulation of 100 nm in thickness and 100 nm in diameter obtained from micromagnetic simulations are shown in Fig. 3 for different positions of the modulation along the nanowire. For the SW (see Fig. 3, right, top) three peaks (peak 1, peak 2 and peak 3) are obtained. Peak 1 (low frequency) is due to magnetization at the ends (top and bottom) of the nanowire, peak 2 (weak, intermediate frequency) is due to the rings that form near the ends (this fine structure appears due to the length of the nanowire),[19] while peak 3 (strong, high frequency) corresponds to the bulk-like mode. The relative magnitudes of the peaks can be explained by the relative volumes affected in the different regions.

The spatial profiles of the magnonic modes are reconstructed to confirm the source of resonant peaks. The temporal Fourier image is calculated for each mesh as $\tilde{m}\left(r_{ijk}, \omega_n\right) = \text{DFT}_t\left(m\left(r_{ijk}, t_n\right)\right)$.[34] These images are essentially the profiles of the magnetization for any particular frequency. The low frequency of the edge modes is due to the fact that they are driven by the magnetostatic field at the edges of the sample. The bulk modes have a higher frequency because they are rather exchange-driven. This effect has been observed previously in rectangular and cylindrical nanowires.[19,20] It is interesting to note

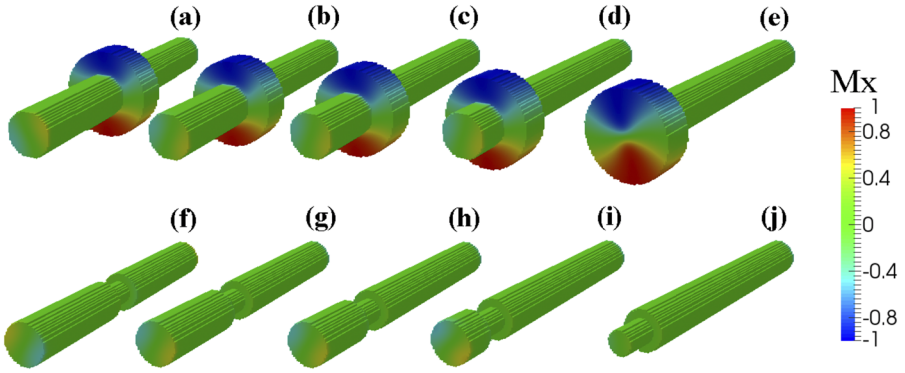

FIG. 2. The equilibrium configurations for WMNs at the given positions for the modulation: (a) 550 nm, (b) 650 nm, (c) 750 nm, (d) 850 nm and (e) 950 nm, and NMNs: (f) 550 nm, (g) 650 nm, (h) 750 nm, (i) 850 nm and (j) 950 nm. The color code on the right represents the magnetization along the x axis (defined in Fig. 1).

that when placing a modulation along the nanowire, the distribution of magnetic charges at the ends is not significantly affected, so peak 1 remains more or less constant regardless of the position in which the modulation is located (see Fig. 3, left).

The exchange interaction tends to align the magnetization in the middle of the wire (near z = 500 nm), giving rise to a high frequency corresponding to peak 3. The intensity of this peak is the highest of all due to the affected area including most of the volume of the system. From Fig. 3, left, we can see that peak 3 remains independent of the position of the modulation along the wire. However, it is interesting to observe how the peak broadens to lower frequencies and decreases its intensity with the presence of the modulation; this is due to the influence of the transverse field of the modulation which disturbs the alignment of the magnetization in the neighboring region producing contributions with slightly lower resonant frequencies. This effect is more notorious when the modulation is centered at 750 nm reflecting the superposition of close resonant frequencies.

Peak 2 appears due to the magnetization near to the ends is not as aligned as that in the middle region of the wire and, therefore, have a slightly lower ferromagnetic resonance frequency. This peak 2 is weak and becomes weaker as the modulation moves from the center towards one of the ends of the wire.

It is interesting to note that the modulation introduces a new peak, which we have defined as peak 4, which is quite intense, greater than peak 1 for all cases except when the modulation reaches one end. One could consider that the modulation of 100 nm in length is the combination of a central cylinder of 50 nm in diameter and a ring of 100 nm in external diameter and 50 nm in internal diameter. Previously we saw that the bulk modes exhibit a high frequency because they depend mainly on the exchange interaction. However, modulation also generates new edges that, as we saw, push the modes at low frequencies mainly due to the magnetostatic field. It is this competition that causes this new peak to appear at an intermediate frequency. When the modulation reaches one of the ends the field at the modulation is even less influenced from the end side, the resulting field is even lower than the previous one and peak 4 moves to lower frequencies (from 6 GHz to 4.8 GHz), while a peak consolidates around 8 GHz.

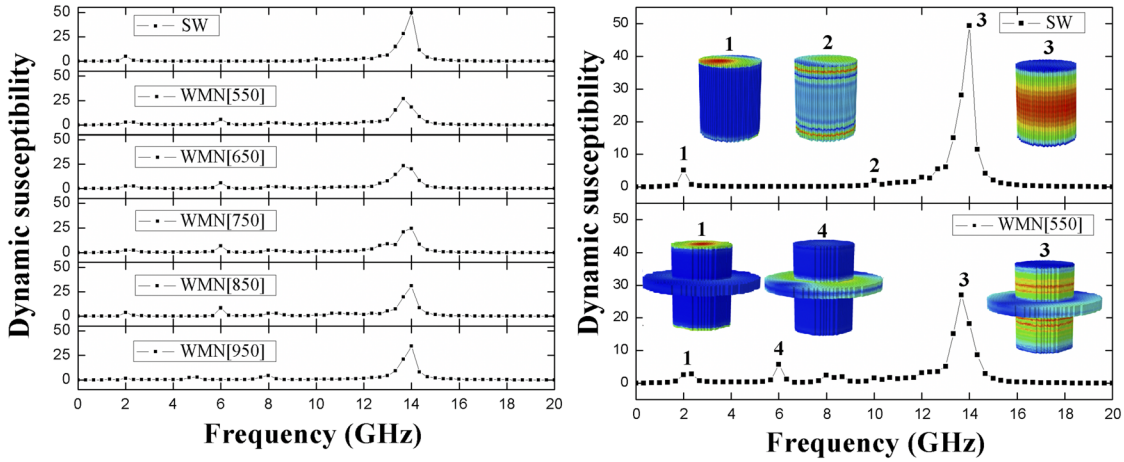

FIG. 3. (Left) Imaginary susceptibility for a WMN at different positions of the modulation along the nanowire. Imaginary susceptibility for a SW (Right, top) and for a WMN with the modulation located at 550 nm (right, bottom). The images represent the spatial distribution of the dynamic susceptibility for each highlighted resonance frequency. The bright part (red) reflects a high spin precession amplitude, the dark (blue) means zero amplitude.

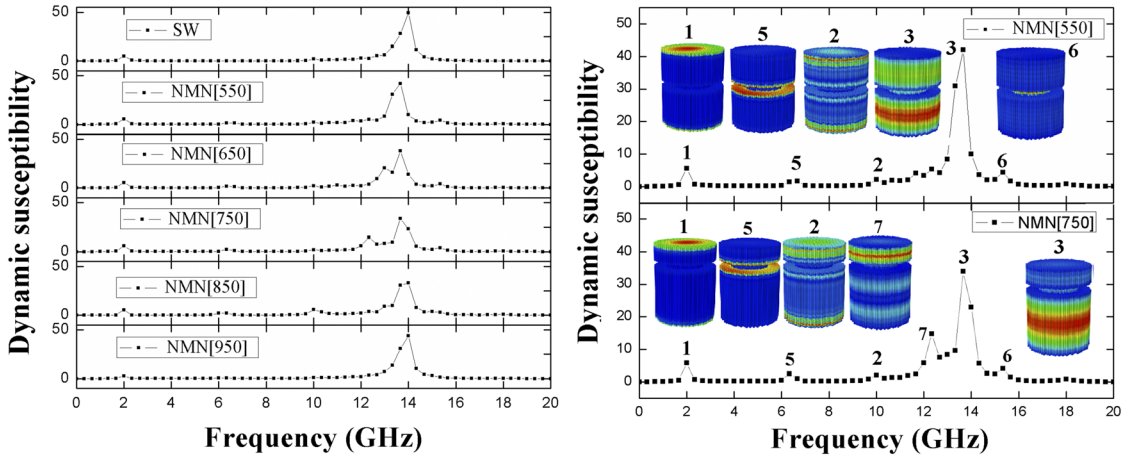

FIG. 4. Imaginary susceptibility for a NMN at different positions of the modulation along the nanowire. Imaginary susceptibility for a NMN with the modulation located at 550 nm (Right, top) and 750 nm (right, bottom). The images represent the spatial distribution of the dynamic susceptibility for each highlighted resonance frequency. The bright part (red) reflects a high spin precession amplitude, the dark (blue) means zero amplitude.

B. Narrow modulated nanowire (NMN)

The dynamic susceptibility for a NMN with a modulation of 100 nm in thickness and 30 nm in diameter obtained from micromagnetic simulations is shown in Fig. 4 for different positions of the modulation along the nanowire. It is interesting to note that, for all these configurations, the system still maintains the peaks 1, 2 and 3 that appear in a SW, and were previously defined (see Fig. 4, left). There are similarities and differences with respect to the previous WMN case. Thus, peak 3 also widens as the modulation moves to one end, but now this phenomenon even produces splitting of the resonance as it can be appreciated for the position at 650 nm. From there the low intensity component moves to lower frequencies as the modulation moves to the end. Finally, this extra peak disappears when the modulation reaches extremities of the wire. The modulation causes the system to behave like two shorter wires interconnected by a thinner wire. When the modulation is in the center, the shorter wires have the same length, so they exhibit a single peak. However, when the modulation moves slightly to one end (i.e. at 550 nm) there is a shorter wire, with slightly lower field producing a broadening of the resonance to lower frequencies. This phenomenon persists as the modulation moves to the end splitting now the resonance due to a shorter wire at lower frequencies (also less intense due to the lower volume involved). When the modulation reaches last possible position, the shorter wire is lost and also its resonance. The contribution of the long wire to peak 3 is now undistinguishable from the SW and the only influence of the modulation is to be found in the lower intensity of peak 1 due to the decrease of the end areas.

Additionally, the presence of a modulation in the NMN generates two new peaks, which we have called peaks 5 and 6. Peak 5 is similar to peak 4 that appears in the WMN, but slightly displaced towards higher frequencies. In fact, the spatial distribution shows that the magnetization reverses from the central ends that appear thanks to the modulation. This peak practically disappears when the modulation reaches one end. On the other hand, peak 6 corresponds to the magnetization reversal process of the modulation, which due to its smaller diameter, the magnetization is more aligned than for the 100 nm wire, reaching a higher localized field that leads to a resonance at higher frequencies not observed in WMN.

IV. CONCLUSIONS

Both WMN and NMN present interesting responses to an excitation by a transverse magnetic pulse. Some of the resonances are similar and other are a property of just one of these systems. The particular values refer to nanowires of 1000 nm in length and 50 nm in diameters. In the case of WMN the modulation is 100 nm thick and 100 nm in diameter; for NWM the modulation is again 100 nm in thickness, but the diameter is only 30 nm. The exciting field was defined in section II.

The starting point is the SW with a weak resonance at 2 GHz due to the ends, a very weak resonance near 10 GHz due to the rings towards the ends and a strong resonance at 14 GHz due to the center of the wire with the higher field and most of the magnetic material. These are referred to as peaks 1, 2 and 3, respectively.

One effect of a wide modulation is to widen peak 3 to lower frequencies. Then two new resonances appear at intermediate frequencies (6 GHz and 8 GHz) which are associated to the flat surfaces of the modulation. The lower frequency resonance shifts to even lower frequencies (4.6 GHz) when the modulation reaches the end position. Consequently peak 1 weakens as it receives contribution from the other end only.

A new peak (peak 6) appears for NMN at frequencies higher than peak 3 (15.6 GHz) and is due to the more efficient alignment of the magnetization within the narrow modulation producing a more intense local field. NMN also present the intermediate resonant frequencies due to the flat surfaces of the modulation but shifted to higher frequencies since the surfaces are now influenced by a stronger field coming from the nearby narrow modulation; they are also weaker than in the case of WMN since the flat area involved

is now lower. Peak 3 broadens to lower frequencies and then splits as the modulation moves to an end.

This opens possibilities of tailoring a desired set of frequencies by controlling the geometrical parameters of the system.

ACKNOWLEDGMENTS

The authors acknowledge financial support from Fondecyt (1150952 and 1150019), Basal Project (FB0807), CONICYT-PCHA/Doctorado Nacional/2014 and Universidad de La Frontera (DI17-0027).

REFERENCES

[1] M. Vázquez, Ed., *Magnetic Nano- and Microwires* (Woodhead Publishing, 2015).
[2] S. Parkin and S. H. Yang, Nat. Nanotechnol. **10**, 195 (2015).
[3] S. Liébana Viñas, R. Salikhov, C. Bran, E. M. Palmero, M. Vázquez, B. Arvan, X. Yao, P. Toson, J. Fidler, M. Spasova, U. Wiedwald, and M. Farle, Nanotechnology **26**, 415704 (2015).
[4] Y. P. Ivanov, M. Vázquez, and O. Chubykalo-Fesenko, J. Appl. Phys. D: Appl. Phys. **46**, 485001 (2013).
[5] R. Hertel, J. Phys. Condens. Matter. **28**, 483002 (2016).
[6] K. Pitzschel, J. M. Montero Moreno, J. Escrig, O. Albrecht, K. Nielsch, and J. Bachmann, ACS Nano **3**, 3463 (2009).
[7] K. Pitzschel, J. Bachmann, S. Martens, J. M. Montero Moreno, J. Kimling, G. Meier, J. Escrig, K. Nielsch, and D. Gorlitz, J. Appl. Phys. **109**, 033907 (2011).
[8] M. S. Salem, P. Sergelius, R. M. Corona, J. Escrig, D. Gorlitz, and K. Nielsch, Nanoscale **5**, 3941 (2013).
[9] F. Tejo, N. Vidal-Silva, A. P. Espejo, and J. Escrig, J. Appl. Phys. **115**, 17D136 (2014).
[10] E. M. Palmero, C. Bran, R. P. Del Real, and M. Vázquez, Nanotechnology **26**, 461001 (2015).
[11] L. A. Rodríguez, C. Bran, D. Reyes, E. Berganza, M. Vázquez, C. Gatel, E. Shoeck, and A. Asenjo, ACS Nano **10**, 9669 (2016).
[12] E. Berganza, C. Bran, M. Jaafar, M. Vázquez, and A. Asenjo, Sci. Rep. **6**, 29702 (2016).
[13] L. C. C. Arzuza, R. López-Ruiz, D. Salazar-Aravena, M. Knobel, F. Berón, and K. R. Pirota, J. Magn. Magn. Mater. **432**, 309 (2017).
[14] J. A. Fernández-Roldán, R. P. del Real, C. Bran, M. Vázquez, and O. Chubykalo-Fesenko, Nanoscale **10**, 5923 (2018).
[15] M. S. Salem, F. Tejo, R. Zierold, P. Sergelius, J. M. Montero Moreno, D. Goerlitz, K. Nielsch, and J. Escrig, Nanotechnology **29**, 065602 (2018).
[16] Y. P. Ivanov, A. Chuvilin, S. Lopatin, and J. Kosel, ACS Nano **10**, 5326 (2016).
[17] C. Bran, E. Berganza, E. M. Palmero, J. A. Fernández-Roldán, R. P. Del Real, L. Aballe, M. Foerster, A. Asenjo, A. Fraile Rodríguez, and M. Vázquez, J. Mater. Chem. C **4**, 978 (2016).
[18] N. Dao, M. J. Donahue, I. Dumitru, L. Spinu, S. L. Whittenburg, and J. C. Lodder, Nanotechnology **15**, S634 (2004).
[19] R. Liu, J. Wang, Q. Liu, H. Wang, and C. Jiang, J. Appl. Phys. **103**, 013910 (2008).
[20] O. Gerardin, J. B. Youssef, H. Le Gall, N. Vukadinovic, P. M. Jacquart, and M. J. Donahue, J. Appl. Phys. **88**, 5899 (2000).
[21] O. Gerandin, H. Le Gall, M. J. Donahue, and N. Vukadinovic, J. Appl. Phys. **89**, 7012 (2001).
[22] J. Wang, B. Zhang, Q. Liu, Y. Ren, and R. Liu, J. Appl. Phys. **105**, 083908 (2009).
[23] C. P. Mu, W. W. Wang, B. Zhang, Q. F. Liu, and J. B. Wang, Physica B **405**, 1325 (2010).
[24] G. Chai, X. Wang, M. S. Si, and D. Xue, Phys. Lett. A **377**, 1491 (2013).
[25] G.-F. Zhang, Z.-X. Li, X.-G. Wang, Y.-Z. Nie, and G.-H. Guo, J. Magn. Magn. Mater. **385**, 402 (2015).
[26] C. Mu, J. Song, J. Xu, and F. Wen, AIP Advances **6**, 065026 (2016).
[27] Y. Peng, G. P. Zhao, F. J. Morvan, S. Q. Wu, and M. Yue, J. Magn. Magn. Mater. **422**, 57 (2017).
[28] C. McKeever, F. Y. Ogrin, and M. M. Aziz, J. Appl. Phys. **121**, 203901 (2017).
[29] T. L. Gilbert, Phys. Rev. **100**, 1243 (1955).
[30] M. J. Donahue and D. G. Porter, OOMMF User's Guide, Version 1.2 a3, 2002, http://math.nist.gov/oommf.
[31] M. Willcox, A. Ding, and Y. Xu, 8th International Vacuum Electron Sources Conference and Nanocarbon, 2010, 11677496.
[32] Q. Wang, L. Jin, X. Tang, F. Bai, H. Zhang, and Z. Zhong, IEEE Trans. Magn. **48**, 3246 (2012).
[33] K. Wagner, S. Stienen, and M. Farle, e-print arXiv:1506.05292v1 [physics. comp-ph].
[34] C. Wen-Bing, H. Man-Gui, Z. Hao, O. Yu, and D. Long-Jiang, Chin Phys. B **19**, 087502 (2010).